

Multiscale Interactions in the Life Cycle of a Tropical Cyclone Simulated in a Global Cloud-System-Resolving Model. Part II: System-Scale and Mesoscale Processes*

HIRONORI FUDEYASU⁺ AND YUQING WANG

International Pacific Research Center, School of Ocean and Earth Science and Technology, University of Hawaii at Manoa, Honolulu, Hawaii

MASAKI SATOH

Atmosphere and Ocean Research Institute, University of Tokyo, Kashiwa, and Japan Agency for Marine Earth Science and Technology, Yokohama, Japan

TOMOE NASUNO

Japan Agency for Marine Earth Science and Technology, Yokohama, Japan

HIROAKI MIURA AND WATARU YANASE

Atmosphere and Ocean Research Institute, University of Tokyo, Kashiwa, Japan

(Manuscript received 22 April 2010, in final form 28 July 2010)

ABSTRACT

The life cycle of Tropical Storm Isobel was simulated reasonably well in the Nonhydrostatic Icosahedral Atmospheric Model (NICAM), a global cloud-system-resolving model. The evolution of the large-scale circulation and the storm-scale structure change was discussed in Part I. Both the mesoscale and system-scale processes in the life cycle of the simulated Isobel are documented in this paper. In the preconditioned favorable environment over the Java Sea, mesoscale convective vortices (model MCVs) developed in the mesoscale convective systems (MCSs) and convective towers with cyclonic potential vorticity (PV) anomalies throughout the troposphere [model vortical hot towers (VHTs)] appeared in the model MCVs. Multiple model VHTs strengthened cyclonic PV in the interior of the model MCV and led to the formation of an upright monolithic PV core at the center of the concentric MCV (primary vortex enhancement). As the monolithic PV core with a warm core developed near the circulation center, the intensification and the increase in horizontal size of the cyclonic PV were enhanced through the system-scale intensification (SSI) process (the secondary vortex enhancement), leading to the genesis of Isobel over the Timor Sea. The SSI process can be well explained by the balanced dynamics.

After its genesis, the subsequent evolution of the simulated Isobel was controlled by both the external influence and the internal dynamics. Under the unfavorable environmental conditions, the development of asymmetric structure reduced the axisymmetric diabatic heating in the inner core and the SSI process became ineffective and the storm weakened. Later on, as the eyewall reformed as a result of the axisymmetrization of an inward-propagating outer spiral rainband, the SSI process became effective again, leading to the reintensification of Isobel. Therefore, the large-scale environmental flow provided the precondition for the genesis of Isobel and the triggering mechanism for subsequent storm-scale structure change as discussed in Part I. The system-scale and mesoscale processes, such as the evolution of MCVs and merging VHTs, were responsible for the genesis, while the eyewall processes were critical to the storm intensity change through the SSI process.

* School of Ocean and Earth Science Technology Publication Number 7985 and International Pacific Research Center Publication Number 714.

⁺ Current affiliation: Faculty of Education and Human Sciences, Yokohama National University, Yokohama, Japan.

Corresponding author address: Dr. Hironori Fudeyasu, Yokohama National University, 79-1 Tokiwadai, Hodogaya-ku, Yokohama, Kanagawa 240-8501, Japan.
E-mail: fude@ynu.ac.jp

1. Introduction

The first global cloud-system-resolving model, that is, the Nonhydrostatic Icosahedral Atmospheric Model (NICAM; Tomita and Satoh 2004; Satoh et al. 2008) with realistic settings and a horizontal grid spacing of 7 km simulated reasonably well the life cycle of Tropical Storm (TS) Isobel formed over the Timor Sea in the austral summer of 2006 (Fudeyasu et al. 2008). In Fudeyasu et al. (2010, hereafter Part I), we focused on the evolution of the large-scale circulation and the storm-scale structure change at different stages in the life cycle of the simulated Isobel. We showed that the westerly wind burst (WWB) over the Java Sea associated with the onset of an Madden–Julian oscillation (MJO) event over the East Indian Ocean played a critical role in the organization of small-/mesoscale convective cyclonic vortices and the genesis of Isobel. The temporary weakening was found to be related to the eyewall breakdown triggered by strong vertical shear and a strong environmental stretching deformation field, whereas the reintensification was associated with the eyewall reformation as a result of the axisymmetrization of an inward-propagating outer spiral rainband. In this paper, we will document the system-scale and mesoscale processes in the life cycle of the simulated Isobel with the focus on processes related to the genesis and intensity change of the simulated Isobel.

The genesis remains the least understood stage in the life cycle of a tropical cyclone (TC) because of the complex scale interactions involved and lack of in situ fine observations over the open ocean where the TC forms. In a preconditioned large-scale environment, the genesis generally involves the mesoscale convective organization, including vortical hot towers (VHTs) and mesoscale convective vortices (MCVs) embedded in mesoscale convective systems (MCSs; e.g., Ritchie and Holland 1997; Simpson et al. 1997; Bister and Emanuel 1997; Hendricks et al. 2004; Montgomery et al. 2006). MCVs generally form in the stratiform precipitation region at midtroposphere and have horizontal scales in the order of 10–100 km (Bister and Emanuel 1997; Ritchie and Holland 1997) and VHTs are deep convective cells with potential vorticity (PV) anomalies throughout the depth of the troposphere on scales of 1–20 km embedded in a MCV (Hendricks et al. 2004; Montgomery et al. 2006). Only when these multiscale systems work cooperatively can a cyclogenesis emerge.

Top down and bottom up are two hypotheses for TC genesis. In the top-down hypothesis, the genesis of MCVs occur within the large-scale stratiform precipitation region in the midtroposphere. The merging of midtropospheric MCVs increases the horizontal scale

and thus the downward penetration of anomalous mid-level cyclonic PV, leading to the cyclogenesis at the surface (Ritchie and Holland 1997; Simpson et al. 1997). The evaporative cooling-induced subsidence from stratiform clouds may also bring the midlevel PV anomaly downward, leading to the genesis of a surface cyclonic vortex (Bister and Emanuel 1997). The bottom-up hypothesis describes the upward development of lower-tropospheric cyclonic vortices via convective processes. In their high-resolution cloud-resolving model simulations, Hendricks et al. (2004) and Montgomery et al. (2006) found that VHTs play an essential role in the genesis of a TC. The merging of multiple VHTs increases the cyclonic vorticity with a low-level vorticity maximum and collective heating can spin up the storm-scale circulation from the lower troposphere upward.

Tory et al. (2006a) explained that top-down and bottom-up hypotheses may operate at two different phases in the TC genesis: top down first during the preconditioning phase and then bottom up in the rapid intensification stage. Earlier studies showed that the MCVs provide the necessary condition for deep convection and initial concentration of cyclonic vorticity (e.g., Zhang and Fritsch 1987; Bartels and Maddox 1991; Zhang and Bao 1996a,b). Thus, the preexisting MCVs may provide favorable environment for the genesis of VHTs and accelerate the merging process of neighboring VHTs. In a recent study, Fang and Zhang (2010, 2011) simulated the initial development of Hurricane Dolly (2008) in a cloud-resolving model. They found that the genesis of Hurricane Dolly was essentially a bottom-up process.

The genesis is generally followed by a rapid intensification during which the storm becomes self-sustaining and capable of intensifying through the system-scale process, such as the wind-induced surface heat exchange (WISHE) mechanism (Ooyama 1969; Rotunno and Emanuel 1987) and the system-scale intensification (SSI) process (Shapiro and Willoughby 1982; Tory et al. 2006a,b, 2007). The SSI process describes the kinematics of TC intensification in which the secondary circulation in response to heat and momentum sources intensifies the slowly evolving primary circulation by bringing high angular momentum toward the inner-core region. This process can be explained well by the balanced dynamics, namely the Sawyer–Eliassen equation (e.g., Eliassen 1951; Shapiro and Willoughby 1982; Schubert and Hack 1982; Holland and Merrill 1984).

The evolution of the inner core and eyewall structure is responsible for the intensity change of a TC (Wang 2002a,b; Wang and Wu 2004). The eyewall forms in an intensifying TC as a convective ring, which coincides with the strongest updrafts and the maximum tangential winds. Although the mechanism for suppression of eyewall

convection is complex (Frank and Ritchie 2001), strong vertical shear of the environmental flow often has a negative effect on eyewall convection and leads to the weakening of a TC. Interaction between the eyewall and strong spiral rainbands can lead to eyewall breakdown and partial eyewall replacement accompanied by an intensity fluctuation of the TC (Wang 2002b). In some special cases, a new convective ring, or concentric eyewall, can form outside the primary eyewall. In such a case, as the outer convective ring propagates inward and amplifies; the inner, primary eyewall weakens and is eventually replaced by the concentric eyewall (Willoughby et al. 1982). The eyewall replacement is usually accompanied by a weakening and then a reintensification of the TC, producing a large fluctuation in TC intensity. Therefore, the eyewall process including its response to any external forcing is crucial to the intensity change of a TC.

The objectives of this study are 1) to describe the mesoscale and system-scale processes in the life cycle of the simulated Isobel in NICAM, 2) to elucidate the physical mechanisms that are responsible for the genesis and intensity change of the simulated Isobel through azimuthal-mean tangential wind budget analysis and the balanced dynamics based on the Sawyer–Eliassen equation, and 3) to synthesize the multiscale interactions involved in the life cycle of the simulated Isobel based on results from both Part I and this part. The rest of the paper is organized as follows. The methodology for diagnostic and budget analyses is described in section 2. Section 3 examines the mesoscale and system-scale processes leading to the genesis of Isobel. The dynamics leading to the subsequent intensity change in Isobel are discussed in section 4. The multiscale interactions in the life cycle of Isobel are synthesized in section 5. The main findings are summarized in the last section.

2. Methodology

Data used in the analyses of this study were the same as those used in Part I, namely from the NICAM simulation with realistic settings at 7-km resolution for a month in the austral summer of 2006, referred to as the MJO experiment (Miura et al. 2007). Details of the simulated tropical storms in the MJO experiment can be found in Fudeyasu et al. (2008; Part I). In this study, the outputs of the MJO experiment, including the snapshots of three-dimensional data at 6-h intervals and 1.5-hourly averaged two-dimensional data at the surface, were used in the analysis.

The azimuthal-mean tangential wind budget was conducted by casting the governing equations into cylindrical coordinates following the moving storm with the storm

motion vector subtracted from the total wind field. The tendency equation for the azimuthal-mean tangential wind can be written as

$$\frac{\partial \bar{v}_t}{\partial t} = -\bar{v}_r \bar{\eta} - \overline{v'_r \eta'} - \bar{w} \frac{\partial \bar{v}_t}{\partial z} - \overline{w' \frac{\partial v'_t}{\partial z}} + \bar{F}_{sg}, \quad (1)$$

where z is height, t is time, v_t is tangential wind, v_r is radial wind, w is vertical velocity, $\eta = f + \zeta$ is absolute vertical vorticity, ζ is relative vertical vorticity, f is the planetary vorticity, and \bar{F}_{sg} is the azimuthal-mean tangential wind tendency due to vertical mixing and surface friction. The overbar denotes the azimuthal mean at a given height, while the prime denotes the deviation (eddy) from the azimuthal mean. The five terms on the right-hand side of Eq. (1) are radial advection of the azimuthal-mean absolute angular momentum by the azimuthal-mean radial wind (mean radial advection), eddy radial flux, vertical advection of azimuthal-mean tangential wind by the azimuthal-mean vertical motion (mean vertical advection), eddy vertical flux, and surface friction and subgrid-scale vertical mixing. The last term is treated as the residual in Eq. (1) in our budget.

To quantify the dynamical processes, we examined the evolution of Ertel's PV defined as

$$PV = \frac{\boldsymbol{\eta} \cdot \nabla \theta}{\rho}, \quad (2)$$

where $\boldsymbol{\eta}$ is the three-dimensional absolute vorticity vector, θ is potential temperature, $\nabla \theta$ is the three-dimensional gradient of potential temperature, and ρ is air density. Here PV is measured in PVU ($1 \text{ PVU} \equiv 1 \times 10^{-6} \text{ m}^2 \text{ s}^{-1} \text{ K kg}^{-1}$).

To investigate the SSI process, the Sawyer–Eliassen equation in pseudoheight Z coordinates is used. The equation can be found in Hendricks et al. (2004), Montgomery et al. (2006), and Fudeyasu and Wang (2011). The forcing terms include momentum forcing and diabatic heating:

$$\bar{F} = -\overline{v'_r \zeta'} - \overline{w' \frac{\partial v'_t}{\partial Z}} + \bar{F}_{sg}, \quad \text{momentum forcing}, \quad (3)$$

$$\bar{Q} = \frac{g}{\theta_0} \left(-\overline{v'_r \frac{\partial \theta'}{\partial r}} - \overline{w' \frac{\partial \theta'}{\partial Z}} + \bar{\theta} \right), \quad \text{diabatic heating}, \quad (4)$$

where terms in the momentum forcing represent the azimuthal-mean eddy radial/vertical flux of the asymmetric momentum and azimuthal-mean subgrid-scale vertical turbulent mixing, including surface friction. In the diabatic heating, g is the acceleration due to gravity (9.81 m s^{-2}), θ_0 is the reference potential temperature

(300 K), the first two terms represent the azimuthal-mean eddy radial/vertical flux of the asymmetric potential temperature, and $\bar{\theta}$ is the azimuthal mean diabatic heating rate. The diabatic heating rate $\dot{\theta}$ for each model grid was calculated by $\dot{\theta} = \partial\theta/\partial t + \mathbf{u} \cdot \nabla\theta$, where \mathbf{u} is the three-dimensional wind vector. In our calculations, if the absolute vorticity $\bar{\eta} = f_0 + \zeta < 0.5f_0$, where f_0 is the planetary vorticity at the cyclone center, we set $\bar{\eta} = 0.5f_0$ to allow the discriminant (Fudeyasu and Wang 2011) to satisfy the elliptical condition. This does not affect the global solution to the Sawyer–Eliassen equation as we tested. The boundary conditions for the Sawyer–Eliassen equation are the same as those of Hendricks et al. (2004) and Montgomery et al. (2006). The computational domain is 0–15 km of pseudoheight in the vertical with 500-m grid interval and 0–504 km in the radial direction with 7-km grid spacing. Variables from the Sawyer–Eliassen calculation were then converted back to the physical height coordinate from the pseudoheight coordinate.

3. Genesis processes

a. Evolution of mesoscale vortices

Figure 1 shows the evolution of PV averaged in a layer between 1 and 8 km above the sea surface and horizontal wind fields at 3-km height. On 25 December 2006, there were little or no areas with cyclonic PV less than -1 PVU in the mid–lower troposphere over the Java Sea (note that cyclonic PV is negative in Southern Hemisphere). During the period from 0000 to 1800 UTC 27 December 2006—that is, the preconditioning stage of the simulated Isobel (see Part I)—the WWB occurred over the Java Sea associated with the onset of an MJO event over the East Indian Ocean. The low-level large-scale cyclonic vorticity and convergence together with high convective available potential energy (CAPE) over the Maritime Continent triggered the development of an east–west elongated rainband over the Java Sea (Figs. 5 and 8 in Part I). From 27 December, the cyclonic PV anomalies with horizontal scales of 50–200 km started to develop in the rainband (Fig. 1). The genesis and development of the cyclonic PV anomalies were associated with the MCSs embedded in the rainband.

Figure 2 shows the vertical structure of PV, relative humidity, vertical velocity, and diabatic heating rate zonally averaged between 114° and 117°E at 0000 UTC 28 December 2006 over the Java Sea. The strong updraft with high relative humidity throughout the depth of the troposphere occurred around 4.5° – 5.5°S (Figs. 2b,c) near the cyclonic shear line of the low-level wind field (not shown). The diabatic heating rate with its maximum at

a height of about 8–10 km was associated with deep convection, whereas that around 4–6-km height near the melting level was mainly associated with stratiform clouds (Fig. 2d). The cyclonic PV anomalies at the 2–5-km heights were indications of the midtropospheric vortex development related to diabatic heating in the stratiform clouds (Fig. 2a), which is consistent with the finding of Raymond and Jiang (1990). We refer to the midtropospheric vortex with horizontal scale more than 50 km as model MCV. During the initial eddy stage from 1800 UTC 27 December to 1800 UTC 28 December, the model MCVs moved southeastward along with the rainband toward the Lesser Sunda Islands (Fig. 1). These MCVs merged and eventually developed into a concentric MCV with the intensified cyclonic PV anomaly near its center, the precursor of the genesis of Isobel.

Figure 3 shows the time–radius cross section of the azimuthal-mean PV averaged between 3–6-km heights and the time–height cross sections of PV averaged within a radius of 301 km following Isobel’s center. Note that before the initial eddy stage the center was fixed as the center of Isobel at 1800 UTC 27 December. The cyclonic PV anomaly appeared first in the mid–lower troposphere between 2- and 5-km heights in the preconditioning stage (Fig. 3b). The organization of MCVs around Isobel’s center was accompanied by cyclonic PV less than -1 PVU with a horizontal scale over 30 km in radius at 1800 UTC 27 December (Fig. 3a). The radius of cyclonic PV increased to 90 km in the early initial eddy stage, but decreased to about 60 km as the cyclonic PV intensified to -5 PVU at the center of the initial eddies in the late initial eddy stage, indicating the contraction of the MCV.

Figure 4 shows a plane view of PV averaged in the mid–lower troposphere between 1- and 6-km heights, the wind fields at 3-km height, and the mid- and lower-level circulation centers (see Part I). By the end of the initial eddy stage, the circulation center tilted toward the northwest and west with height, which is consistent with the strong easterly vertical shear (Figs. 8c and 10 in Part I). At 0000 UTC 28 December, a few strong cyclonic PV anomalies with central values less than -4 PVU and radii less than 40 km were embedded in the MCVs. The centers of these small-scale vortices did not coincide with the circulation centers at that time. Figure 5 shows the vertical structure of PV anomalies along the segment A–C labeled at 0000 UTC 28 December in Fig. 4. The PV anomalies marked A and B in Fig. 4 had high cyclonic PV values less than -9 and -6 PVU, respectively, up to 11-km height, whereas the PV anomaly C had high cyclonic PV in the lower troposphere (Fig. 5a). The PV anomalies A and B were accompanied by strong updrafts (Fig. 5c). Strong updraft southeast of the PV

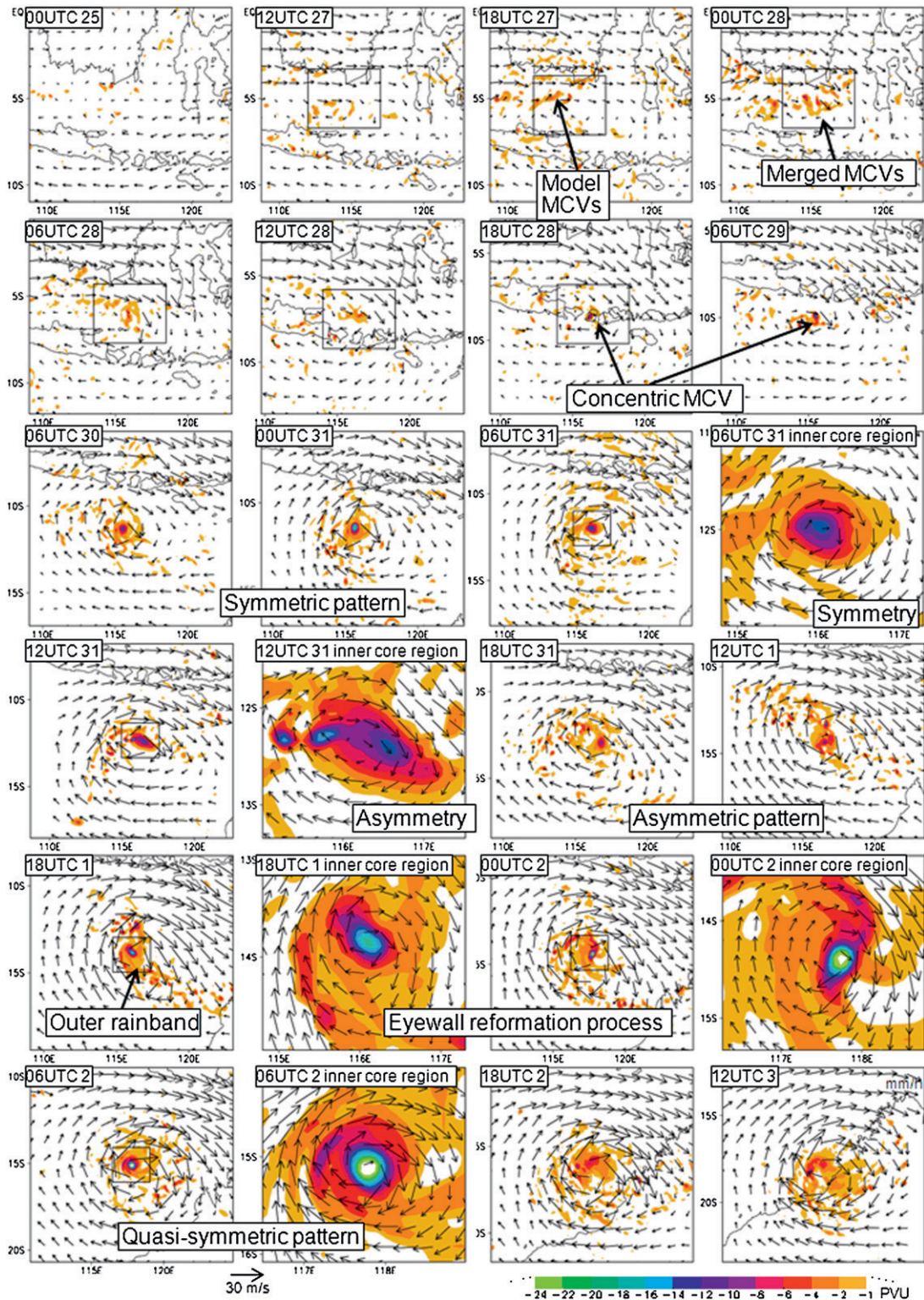


FIG. 1. PVU (shaded) averaged in the layer between 1- and 8-km heights above the sea surface and horizontal winds (vector) at 3-km height. Regions with cyclonic vorticity less than -1 PVU are shaded. The focused views on the inner-core PV are shown at 0600 and 1200 UTC 31 Dec 2006, 1800 UTC 1 Jan 2007, and 0000 and 0600 UTC 2 Jan 2007.

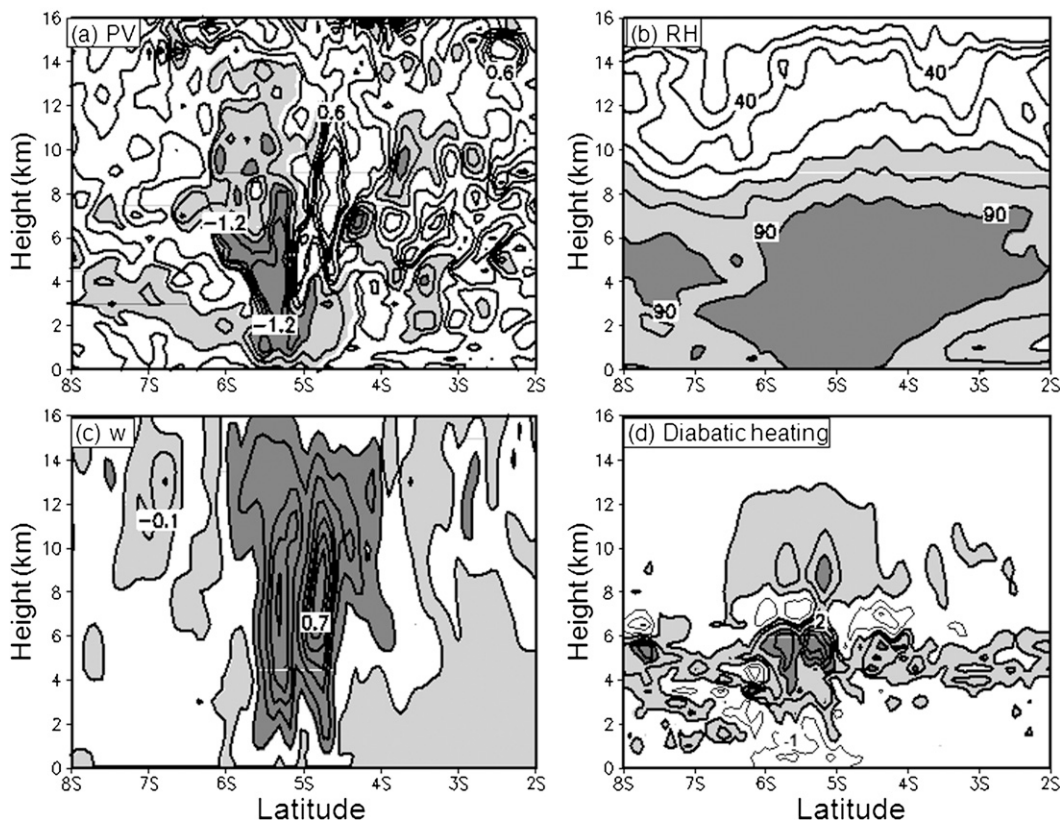


FIG. 2. Vertical-meridional cross sections of (a) PVU, (b) relative humidity (%), (c) vertical velocity (m s^{-1}), and (d) diabatic heating rate (10^{-3} K s^{-1}) zonally averaged between 114° and 117°E at 0000 UTC 28 Dec 2006. In (a), the contour interval is 0.3 PVU, and regions less than -0.3 PVU (-0.9 PVU) are lightly (heavily) shaded. In (b), the contour interval is 10%, and the regions greater than 70% (90%) are lightly (heavily) shaded. In (c), the contour interval is 0.1 m s^{-1} and regions greater than 0.1 m s^{-1} (less than 0 m s^{-1}) are heavily (lightly) shaded. In (d), the contour interval is $1.0 \times 10^{-3} \text{ K s}^{-1}$ and regions greater than $0.1 \times 10^{-3} \text{ K s}^{-1}$ ($2.0 \times 10^{-3} \text{ K s}^{-1}$) are lightly (heavily) shaded.

anomaly C was associated with the PV anomaly D (Fig. 4), which tilted northward with height. Warm anomalies of about 4 K (defined as the temperature deviation from the reference temperatures averaged at the same height in a region of 30°S – 0° , 80° – 140°E at 0000 UTC 23 December 2006) occurred around 10-km height, an indication of active convection with each cyclonic PV anomaly (Fig. 5e). The warm anomalies, however, were too weak to have signals in the sea level pressure (SLP) field (Fig. 5g).

These deep cyclonic PV anomalies with a horizontal scale of about 40 km are associated with deep convection, very similar to those associated with VHTs as discussed in Hendricks et al. (2004) and Montgomery et al. (2006). However, the horizontal scale of the vortices in the simulation is larger than VHTs derived from observations (Reasor et al. 2005; Sippel et al. 2006), mainly because of the relatively coarse model resolution. In our following discussions, we refer to the deep, cyclonic PV

anomalies embedded in model MCVs as model VHTs or convective PV anomalies because they exhibited vortex interactions very similar to the observed VHTs in the initial eddy stage of the simulated Isobel.

The multiple model VHTs were identifiable in the model MCVs until 0600 UTC 28 December, while their number decreased by the end of the initial eddy stage (Fig. 4). A monolithic PV core with peak cyclonic PV less than -14 PVU formed near the center of the concentric MCV at 1800 UTC 28 December. Because the lifetime of convective clouds is generally less than 1–2 h, each VHT could not be tracked with the 6-hourly output of the MJO experiment. However, surface relative vorticity and rainfall derived from 1.5-hourly output showed the merging of VHTs in the organized convective rainband (not shown). The merging of multiple cyclonic PV anomalies formed a monolithic PV core, which is consistent with the finding of Tory et al. (2006b, 2007).

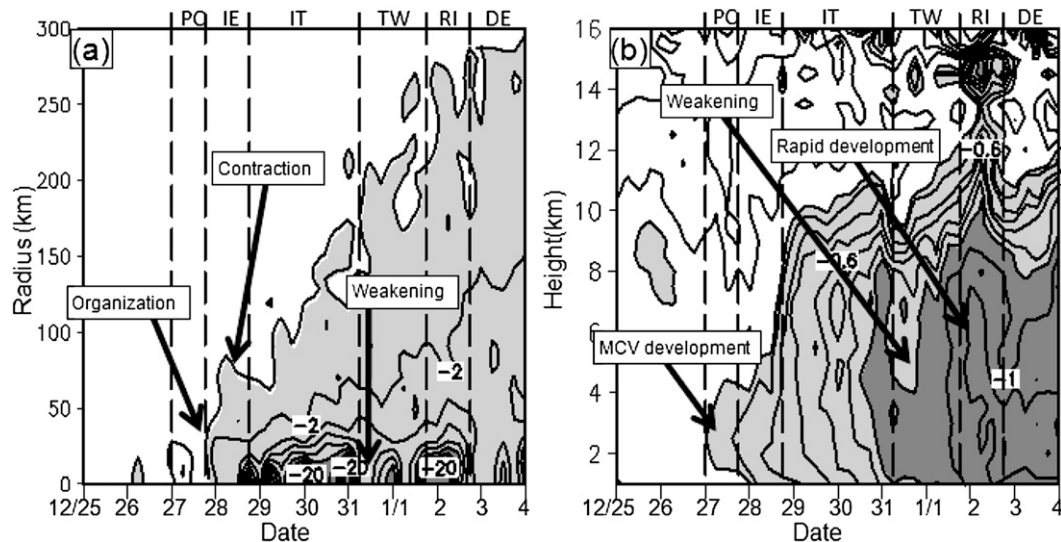


FIG. 3. (a) Time evolution of the azimuthal-mean PVU as a function of radius averaged in a layer between 3- and 6-km heights with contour interval of 1 PVU and regions less than -1 PVU (-6 PVU) lightly (heavily) shaded. (b) Time–height cross section of PVU averaged within a radius of 301 km from Isobel’s center with contour interval of 0.1 PVU and regions less than -0.2 PVU (-0.8 PVU) lightly (heavily) shaded.

Figure 5b shows the vertical structure of the monolithic PV core with a peak cyclonic PV of -19 PVU. The monolithic PV core was accompanied by strong updrafts over 8 m s^{-1} (Fig. 5d). Although the peak cyclonic PV anomaly of the monolithic PV core at 1800 UTC 28 December was about 2–3 times that of previous VHTs at 0000 UTC 28 December, the horizontal scale of the monolithic PV core remained small and was similar to those of previous VHTs. The warm anomalies intensified in the upper troposphere with the maximum temperature anomaly of over 8 K and expanded radially outward (Fig. 5f), resulting in low pressure at the surface (Fig. 5h). Note that the center of the monolithic PV core now coincided with the circulation center (Fig. 4) and a vertically aligned, deep cyclonic circulation developed. The system thus possessed the typical structure of a TC, namely the genesis of Tropical Storm Isobel.

b. Storm-scale process

To evaluate the physical mechanism responsible for the genesis of the simulated Isobel in the initial eddy stage, we conducted the budget and diagnostic analyses for two times: 0000 UTC 28 December (the early initial eddy stage) when multiple VHTs were active, and 1800 UTC 28 December (the late initial eddy stage) after the formation of monolithic PV core. Figures 6 and 7 show the azimuthal-mean radial and tangential winds, vertical velocity, the time tendency in tangential winds, and terms that contribute to the azimuthal-mean tangential wind budget in Eq. (1) for the two times,

respectively. The storm centers used in the calculation for symmetric/asymmetric components were defined as the 850-hPa circulation center at 0000 UTC 28 December and the mass center (see Part I) at 1800 UTC 28 December (also in Figs. 8–12).

In the early initial eddy stage, the weak azimuthal-mean inflow occurred in the midtroposphere with the peak at 4-km height between radii of 150–300 km and weak outflow occurred in a relatively deep layer in the upper troposphere (Fig. 6a). Weak cyclonic tangential winds extending to large radii appeared below 7-km height (Fig. 6c) and weak updrafts occurred between radii of 30–50 km in the mid–upper troposphere (Fig. 6b). In the late initial eddy stage, strong updrafts occurred throughout the depth of the troposphere within a radius of about 30 km from the center (Fig. 7b). Tangential winds more than 8 m s^{-1} occurred in the lower troposphere extending radially outward with the maximum in the boundary layer between the radii of 15 and 50 km (Fig. 7c). There were two inflow layers: a strong one in the boundary layer below 2 km and a weak one in the midtroposphere with a weak outflow in between that peaked at around 4-km height (Fig. 7a).

The azimuthal-mean tangential wind increased with time throughout the depth of the troposphere within a radius of about 250 km with the maximum increase in the mid–lower and upper troposphere between the radii of 20 and 100 km in the early initial eddy stage (Fig. 6d). The spinup of the azimuthal-mean tangential wind resulted from the mean radial/vertical advectations of absolute angular momentum in the mid–lower troposphere and

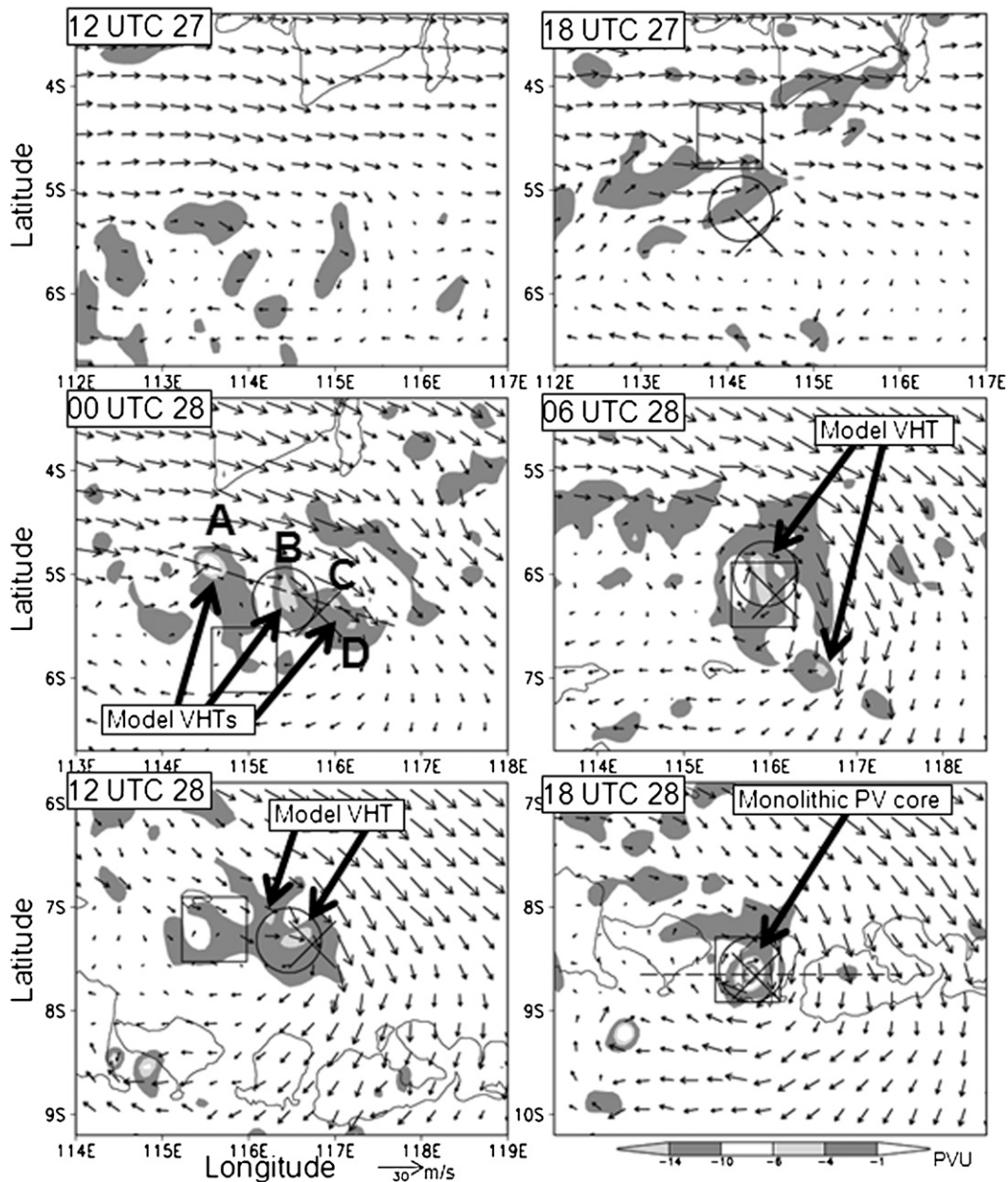


FIG. 4. As in Fig. 1, but for PVU (shaded) averaged in the layer between 1- and 6-km heights with different shading scales shown at the bottom of the lower-right. Cross, circle, and square represent the circulation centers at 850, 700, and 500 hPa, respectively.

the eddy fluxes in both the upper and lower troposphere (Figs. 6e,f). In the late initial eddy stage, areas with the spinup of tangential wind expanded to large radii (Fig. 7d). The maximum increase occurred from the surface up to 12-km height in the inner-core region and was mainly contributed to by the mean advectons (Fig. 7e). Contribution by the eddy process to the azimuthal-mean tangential wind budget was generally small in the late initial eddy stage (Fig. 7f).

Since the mean advection associated with the azimuthal-mean radial and vertical winds (secondary circulation) is responsible for the spinup of the azimuthal-mean primary circulation, it is our intent to examine what contributed to the azimuthal-mean secondary circulation during the initial eddy stage of the simulated Isobel. Figures 8a,b show the radius-vertical cross section of the azimuthal-mean diabatic heating rate (the dominant forcing term in the Sawyer-Eliassen equation, as will be

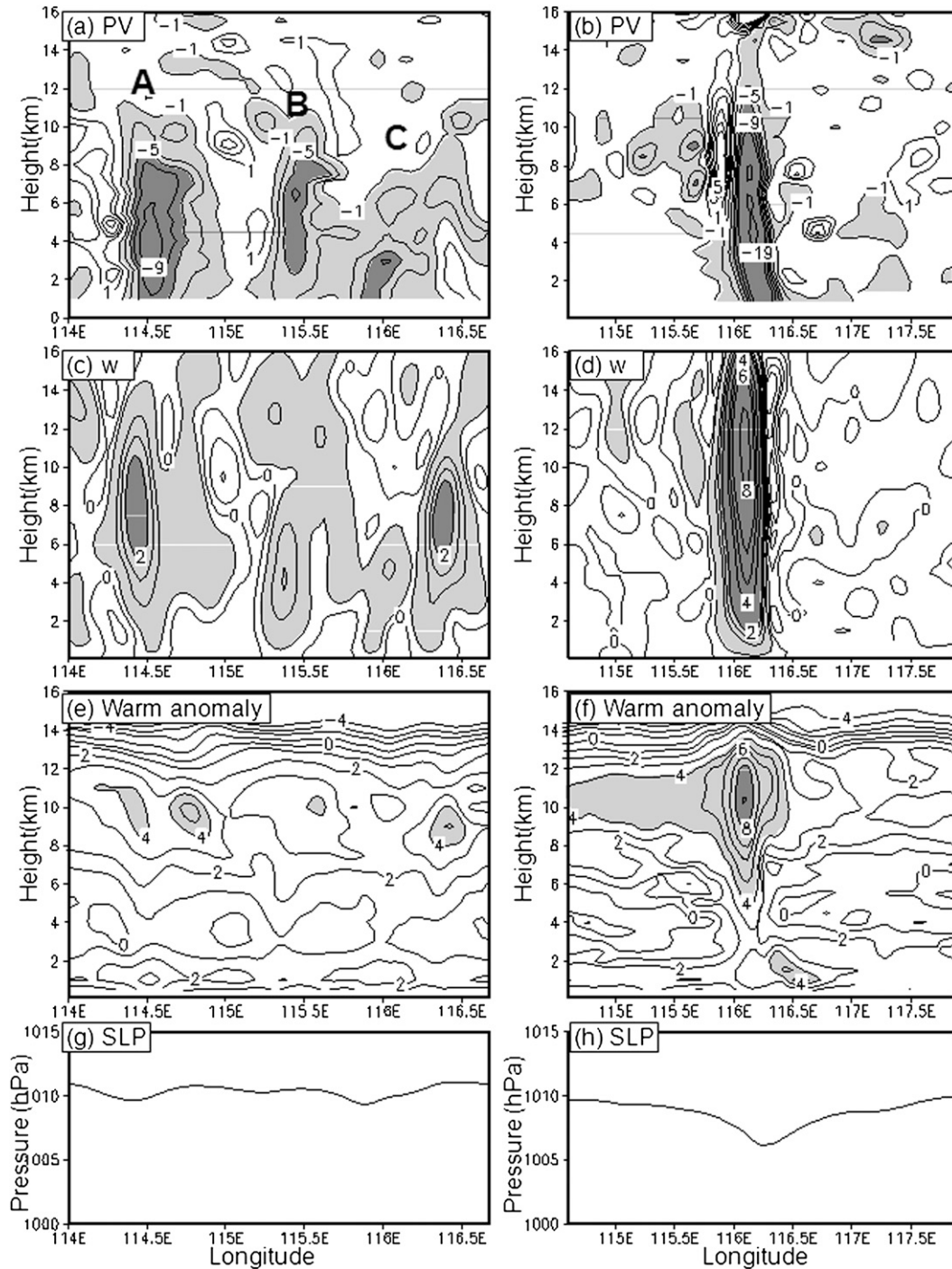


FIG. 5. Vertical cross sections of (a),(b) PVU; (c),(d) vertical velocity (m s^{-1}); (e),(f) warm anomalies (K); and (g),(h) sea level pressure (hPa) at (left) 0000 and (right) 1800 UTC 28 Dec 2006. Locations of the cross sections are marked as line segments in Fig. 4. The contour interval is 1 PVU and regions less than -1 PVU (-5 PVU) are lightly (heavily) shaded in (a),(b). The contour interval is 0.5 m s^{-1} and regions more than 0.5 m s^{-1} (2.0 m s^{-1}) are lightly (heavily) shaded in (c),(d). The contour interval is 1 K and the regions more than 4 K (8 K) are lightly (heavily) shaded in (e),(f). The warm anomaly was calculated as the difference of potential temperature from the reference potential temperature averaged in 30°S – 0° and 80° – 140°E at 0000 UTC 23 Dec 2006.

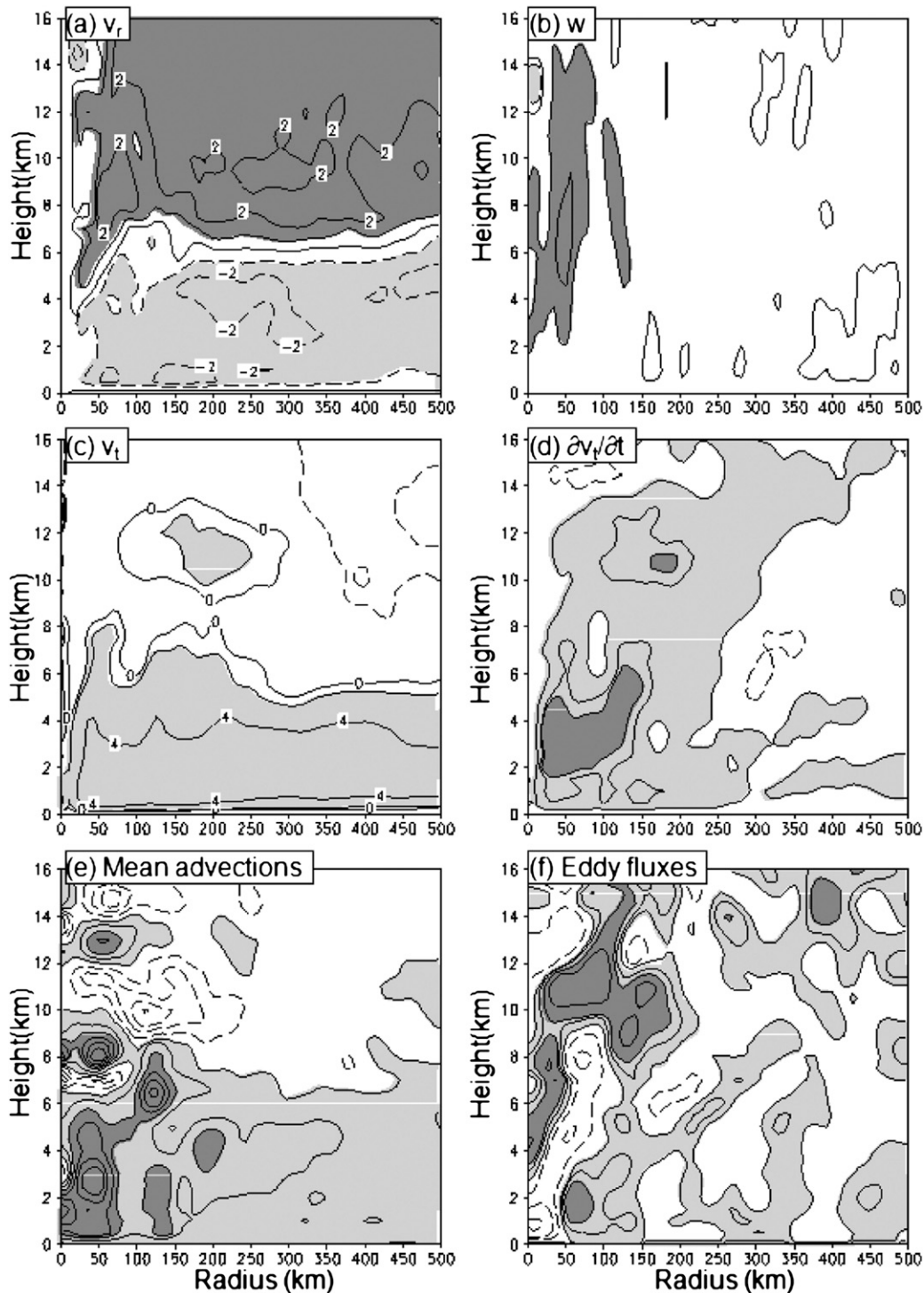


FIG. 6. Azimuthal-mean (a) radial wind (m s^{-1}), (b) vertical velocity (m s^{-1}), (c) tangential wind (m s^{-1}), (d) the time tendency in tangential wind (m s^{-2}) estimated based on term on left-hand side of Eq. (1), (e) mean radial and vertical advective fluxes, and (f) eddy radial and vertical fluxes estimated based on terms on right-hand side of Eq. (1) at 0000 UTC 28 Dec 2006. The contours are at 0, ± 1 , ± 2 , ± 5 , and $\pm 10 \text{ m s}^{-1}$ and regions greater than 1 m s^{-1} (less than 1 m s^{-1}) are heavily (lightly) shaded in (a). The contour interval is 0.2 m s^{-1} and regions greater than 0.2 m s^{-1} (less than -0.05 m s^{-1}) are heavily (lightly) shaded in (b). The contour interval is 2 m s^{-1} and regions greater than 2 m s^{-1} (10 m s^{-1}) are lightly (heavily) shaded in (c). The contour interval is $1 \times 10^{-4} \text{ m s}^{-2}$ and regions greater than 0 m s^{-2} ($2 \times 10^{-4} \text{ m s}^{-2}$) are lightly (heavily) shaded in (d)–(f). Solid contours denote positive values and dashed contours, negative values.

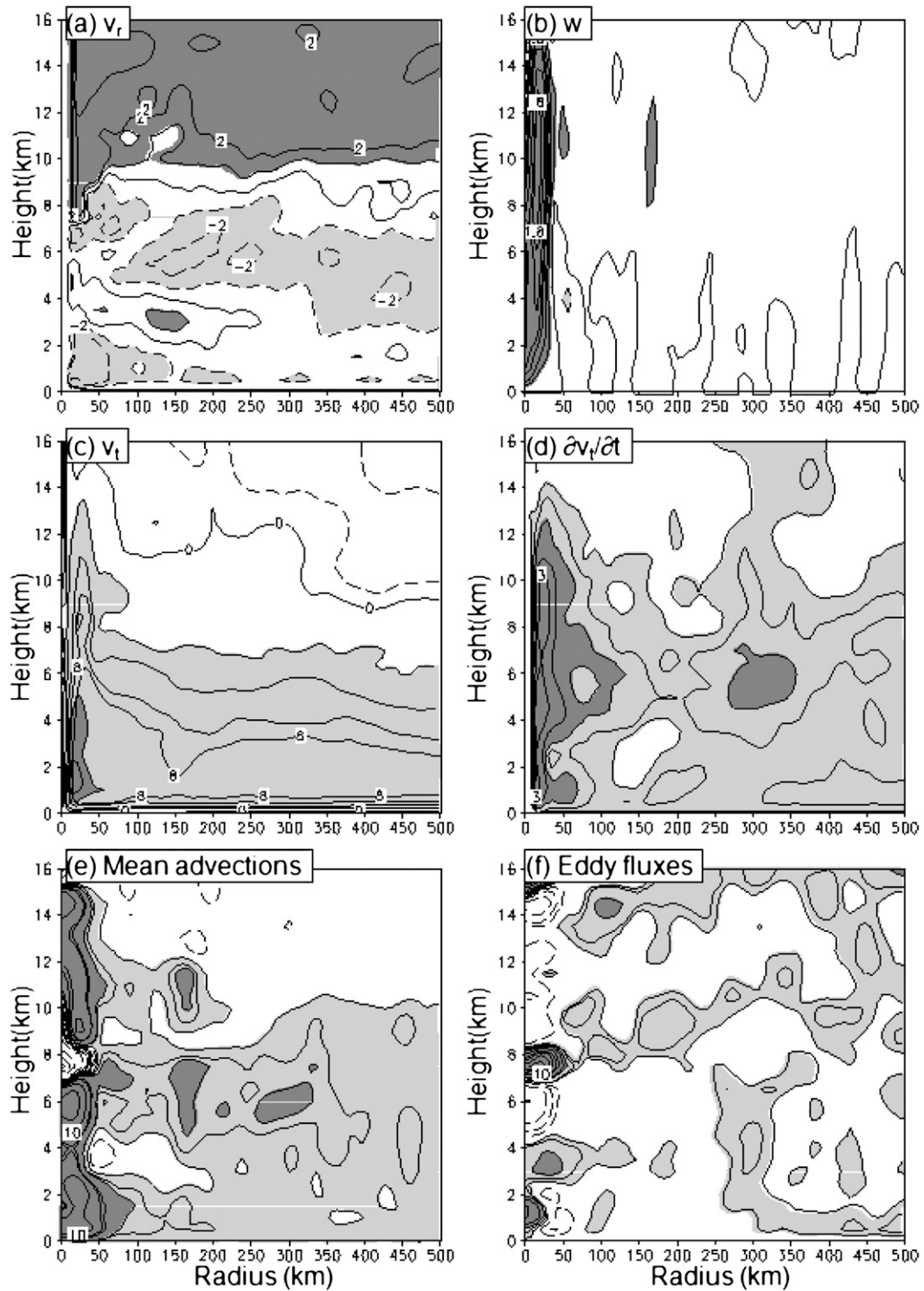


FIG. 7. As in Fig. 6, but at 1800 UTC 28 Dec 2006.

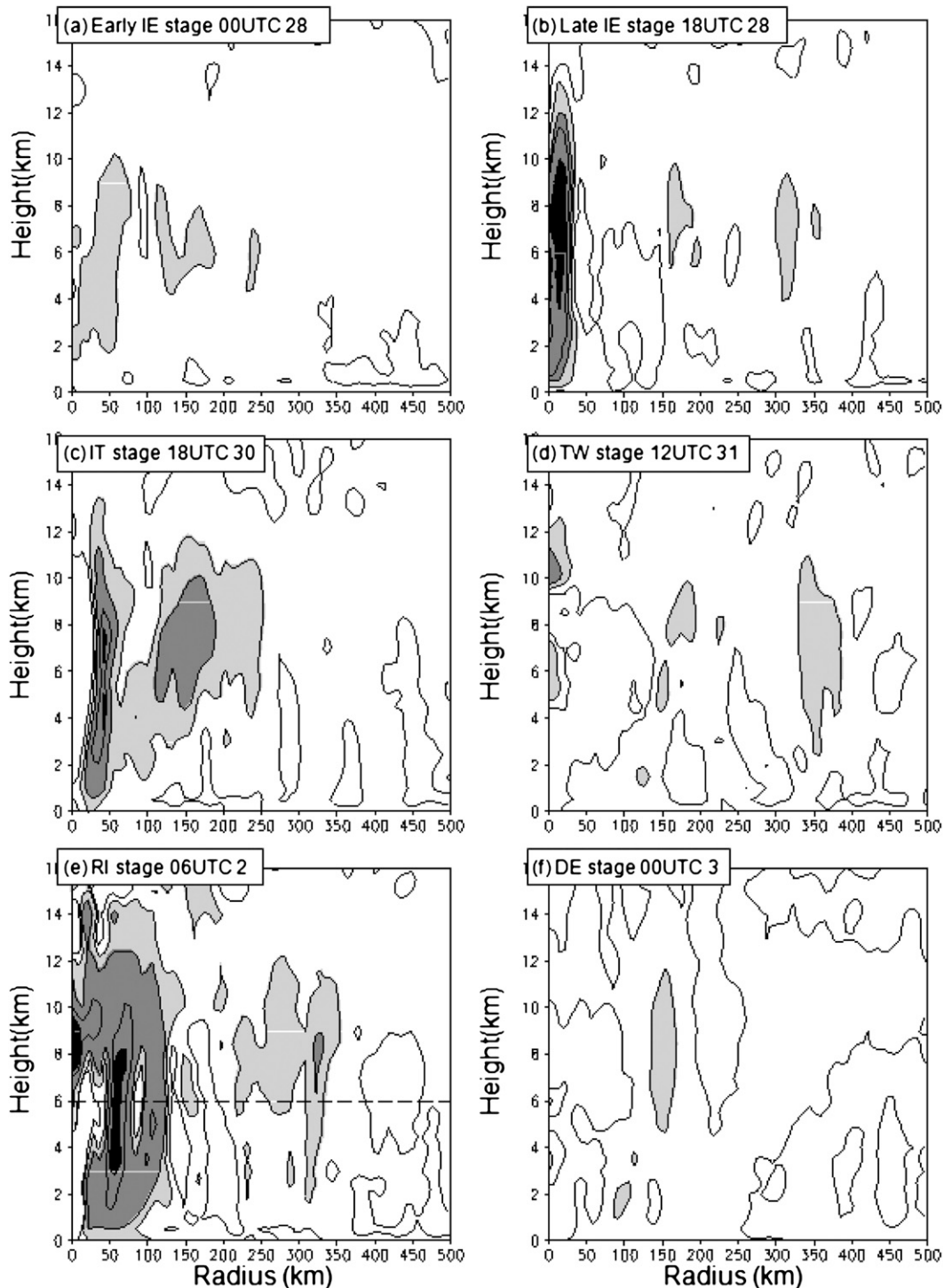


FIG. 8. Azimuthal-mean diabatic heating rate (K s^{-1}) at (a) 0000 UTC 28 Dec, (b) 1800 UTC 28 Dec, (c) 1800 UTC 30 Dec, (d) 1200 UTC 31 Dec 2006, (e) 0600 UTC 2 Jan, and (f) 0000 UTC 3 Jan 2007. The contour interval is $1 \times 10^{-4} \text{ K s}^{-1}$. Regions greater than $4 \times 10^{-4} \text{ K s}^{-1}$ are filled and regions greater than $2 \times 10^{-4} \text{ K s}^{-1}$ are heavily shaded, while regions greater than $1 \times 10^{-4} \text{ K s}^{-1}$ are lightly shaded. Dashed horizontal lines represent the height of 6 km used in the sensitivity calculations in (e).

discussed later) in the early and late initial eddy stages, respectively. The azimuthal-mean diabatic heating rate was negligible in the early initial eddy stage (Fig. 8a), but became large within a radius of 30 km in the late initial eddy stage (Fig. 8b). The latter was associated with convective heating in the strong updraft in the monolithic PV core (Fig. 5). The secondary circulation diagnosed from the Sawyer–Eliassen equation for the early initial eddy stage was quite different from the model simulation (not shown), indicating that the azimuthal-mean secondary circulation at the early initial eddy stage cannot be explained by the balanced dynamics. On the other hand, the azimuthal-mean secondary circulation for the late initial eddy stage was reproduced reasonably well using the Sawyer–Eliassen equation (Figs. 7a,b and 9a,b), although considerable differences exist in the region outside about 200–300-km radii and in the upper troposphere. This is consistent with Hendricks et al. (2004) and Montgomery et al. (2006), who also showed that the storm-scale secondary circulation in the genesis stage was nearly in both gradient wind and thermal wind balances and could be well explained by the balanced dynamics using the Sawyer–Eliassen equation.

Since the Sawyer–Eliassen equation is linear, its solution is additive. This allows us to understand which forcing process is responsible for the secondary circulation at the late initial eddy stage. We thus performed two calculations: in one calculation only the azimuthal-mean diabatic heating forcing term in the last term on the right-hand side of Eq. (4) (see Fig. 8) was included in solving the Sawyer–Eliassen equation and in the other calculation only the eddy terms, namely the first and the second terms in Eqs. (3) and (4), were included. The results showed that the secondary circulation at the late initial eddy stage was mostly driven by the azimuthal-mean diabatic heating (not shown). That is, as a monolithic PV core with warm core developed at the circulation center, the secondary circulation was enhanced by convective heating in the monolithic PV core, contributing to the intensification of the primary circulation.

4. Intensity change

After Isobel passed over the Lesser Sunda Islands at 1800 UTC 28 December, the concentric MCV with the monolithic PV core developed into Tropical Storm Isobel over the Timor Sea, which then intensified from 1800 UTC 28 December to 0600 UTC 31 December (Fig. 1). The azimuthal-mean cyclonic PV averaged between 3- and 6-km heights increased up to -20 PVU in the inner core of the simulated Isobel (Fig. 3a). The cyclonic PV less than -1 PVU extended radially outward up to 150 km from the storm center, indicating an

increase in the horizontal scale of the simulated Isobel. The outward expansion of high cyclonic PV was closely related to the formation of an outer spiral rainband (Figs. 5 and 12 in Part I). By 1800 UTC 30 December the simulated Isobel showed the typical structure of a mature TC with the maximum tangential wind near the surface under the eyewall (Fig. 10c), updrafts in the eyewall and outer spiral rainbands, subsidence in the eye (Fig. 10b), inflow in the mid–lower troposphere and outflow both in the core just above the inflow boundary layer and in the upper troposphere (Fig. 10a). Convective heating occurred through the depth of the troposphere between radii of 20 and 40 km in the eyewall and in the mid–upper troposphere in outer rainbands between radii of 100 and 250 km (Fig. 8c).

The intensification of the primary circulation occurred through the depth of the troposphere but most strongly in the inner-core region in the intensifying stage (Fig. 10d). The inner-core intensification was mainly attributed to the mean advections in the lower and upper troposphere and to eddy fluxes in the midtroposphere (Figs. 10e,f). As the case in the later initial eddy stage, now the azimuthal-mean radial and vertical winds were captured well by the solution of the Sawyer–Eliassen equation although some noise existed in the upper-tropospheric outflow (Figs. 9c,d). Therefore, the intensification of the primary circulation in the inner-core region can be well explained by the balanced dynamics, namely the SSI process.

In the temporally weakening stage from 0600 UTC 31 December 2006 to 1800 UTC 1 January 2007, the intensification of the simulated Isobel was interrupted by the influences of strong vertical shear first and a strong environmental stretching deformation in the mid–lower troposphere later as discussed in Part I. At 0600 UTC 31 December by the end of the intensifying stage, a symmetric PV monopole structure in the inner-core region appeared with a peak of -14 PVU (Fig. 1). Isobel experienced an abrupt structure change at 1200 UTC 31 December with the central PV monopole split into two areas: one to the west and one to the east of Isobel's center. The asymmetric structure of the inner-core PV remained until 1200 UTC 1 January 2007. The decay of the symmetric structure in Isobel during the early temporally weakening stage was accompanied with the westward tilt of the vertical vorticity center due to the effect of strong easterly vertical shear as discussed in Part I, which is similar to the PV pattern in the case of TC Chris discussed in Tory et al. (2006b).

It is interesting to see that the weakening of the primary circulation started from the upper troposphere in the core region (Figs. 3b and 11c), consistent with the finding of Frank and Ritchie (2001), who found that their simulated storm weakened from the top down in

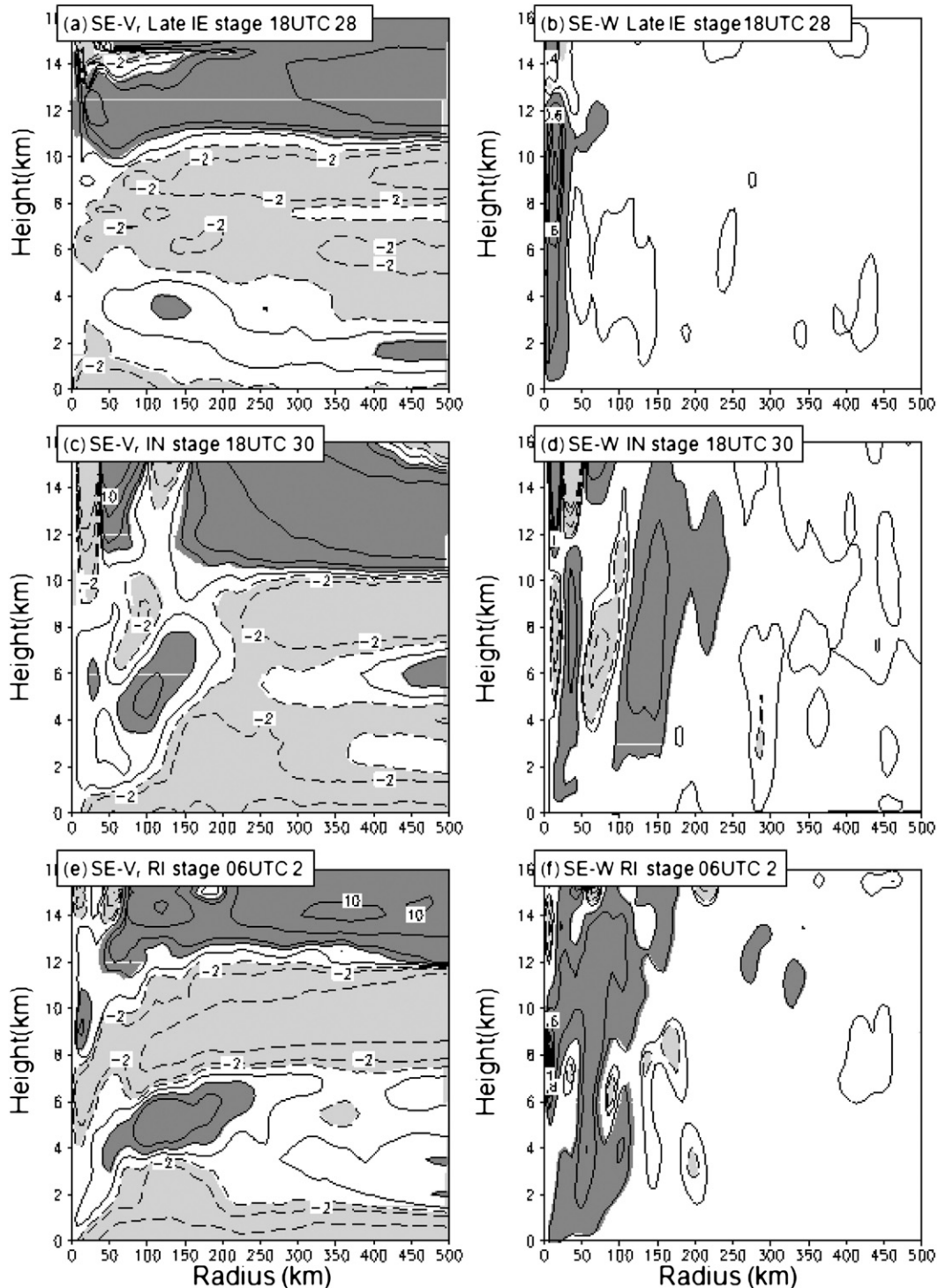


FIG. 9. Azimuthal-mean (a),(c),(e) radial winds (m s^{-1}) and (b),(d),(f) vertical velocity (m s^{-1}) derived from the Sawyer–Eliassen equation at (a),(b) 1800 UTC 28 Dec 2006 in the same domain as in Fig. 7, at (c),(d) 1800 UTC 30 Dec 2006 in the same domain as in Fig. 10, and at (e),(f) 0600 UTC 2 Jan 2007 in the same domain as in Fig. 12. Contours are at 0, ± 1 , ± 2 , ± 5 , and $\pm 10 \text{ m s}^{-1}$ and regions greater than 1 m s^{-1} (less than 1 m s^{-1}) are heavily (lightly) shaded in (a), (c), and (e). The contour interval is 0.2 m s^{-1} and regions greater than 0.2 m s^{-1} (less than -0.05 m s^{-1}) are heavily (lightly) shaded in (b),(d), and (f). Solid contours denote positive values; dashed contours, negative values.

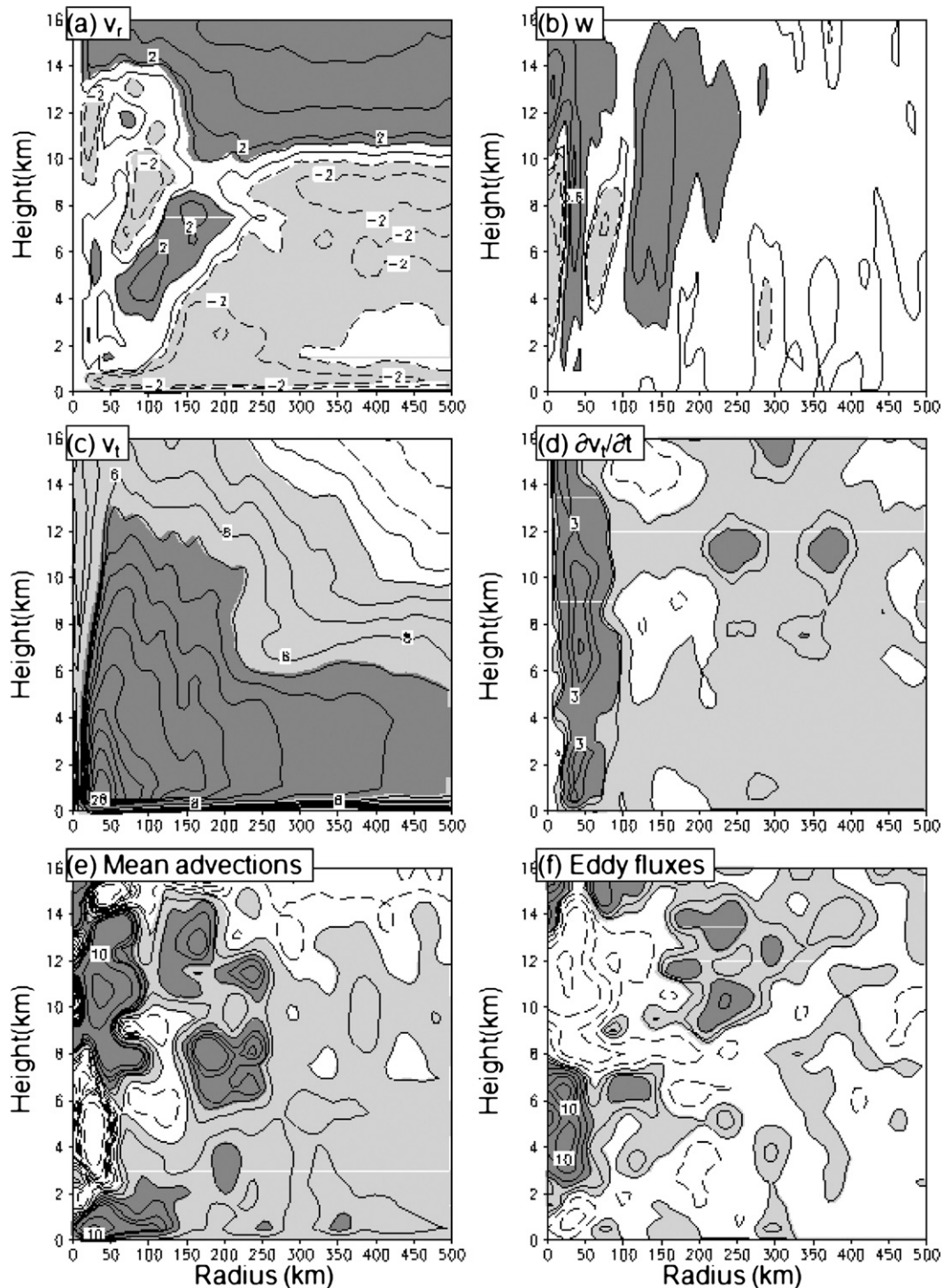


FIG. 10. As in Fig. 6, but at 1800 UTC 30 Dec 2006.

a vertical shear environment. The radial wind was exhibited by a deep outflow layer up to a radius of about 350 km between 2- and 4-km heights with a deep inflow layer between 5- and 12-km heights immediately below

the upper-tropospheric outflow (Fig. 11a). The mid-upper-tropospheric inflow implied a convergence into the eye and eyewall region, consistent with a subsidence in the inner core below about a 10-km height (Fig. 11b).

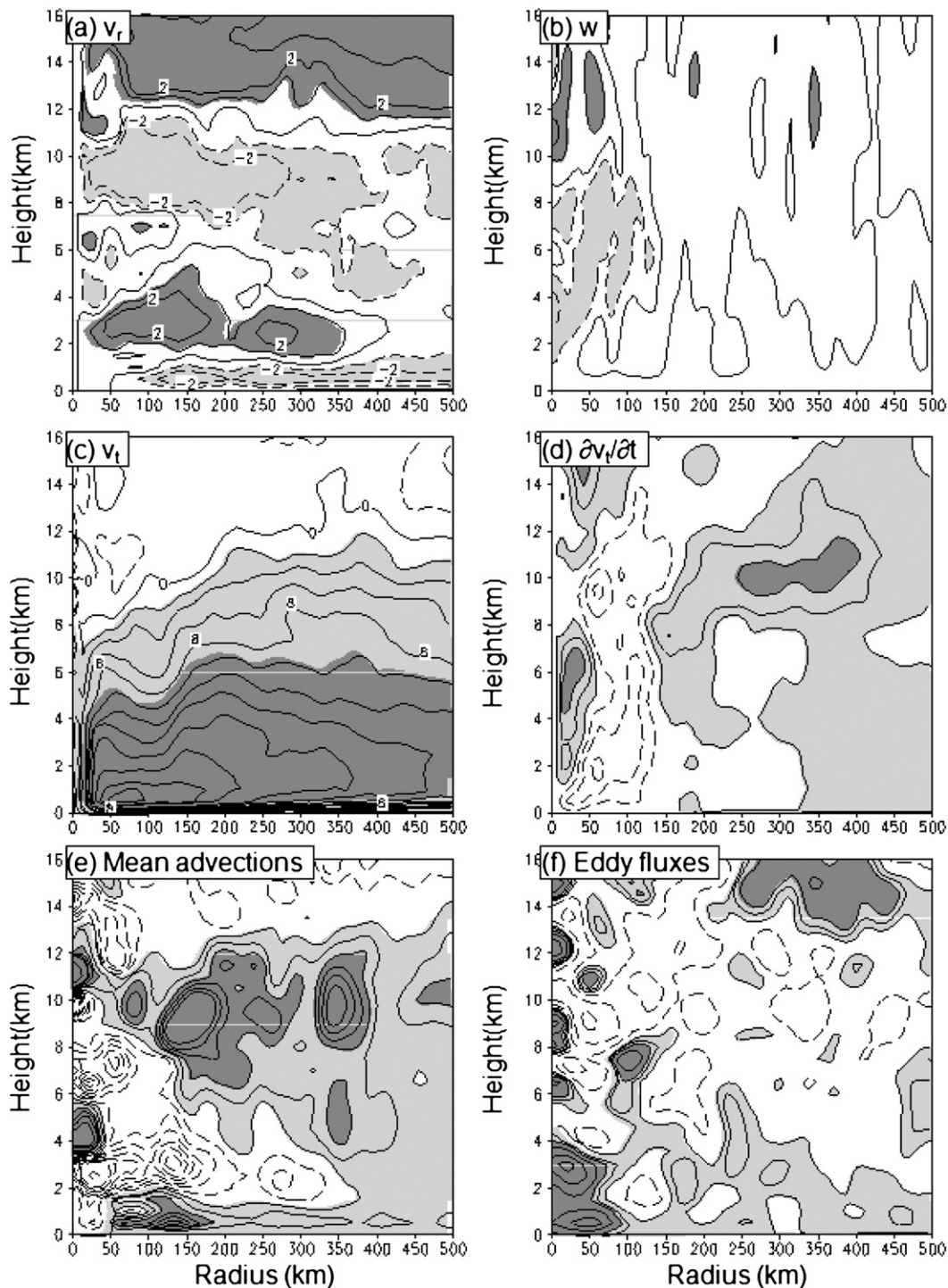


FIG. 11. As in Fig. 6, but at 1200 UTC 31 Dec 2006.

Such a secondary circulation led to a spindown of the tangential wind in the mid-lower troposphere and a spinup of the tangential wind in the mid-upper-tropospheric inflow layer mainly outside the inner-core region (Figs. 11d,e). Eddies played a role in spinning

down the primary circulation except for in the lower troposphere and in the core region (Fig. 11f). As a result, the azimuthal-mean tangential wind decreased in a deep layer below 12-km height within a radius of about 100 km except for a small area in the eye between 1- and 8-km

heights (Fig. 11d), an indication of inward mixing by both the azimuthal-mean inflow and eddy transport (Figs. 11e,f). Consistent with the inflow immediately below the upper-tropospheric outflow, there was a spinup of tangential wind outside the core region between 7- and 12-km heights (Fig. 11d). Note that the azimuthal-mean diabatic heating rate in the inner core of the storm was almost dismissed in the weakening stage (Fig. 8d). The SSI process became ineffective and the storm weakened.

Later on, the simulated Isobel experienced an eyewall reformation as discussed in Part I. This led to a re-intensification of the storm from 1800 UTC 1 January to 1800 UTC 2 January 2007. At 1800 UTC 1 January, a high cyclonic PV band was initiated outside the eyewall (Fig. 1) in an outer rainband south of Isobel's center (Fig. 5 in Part I). The cyclonic PV band associated with the rainband displayed a hooklike structure extending southeastward from the core of Isobel (Fig. 1). The PV band then spiraled cyclonically inward, merged into the inner-core PV from the north by 0000 UTC 2 January, and enhanced the cyclonic PV in the inner core. This was accompanied with a reformation of the quasi-symmetric PV monopole structure with a peak cyclonic PV less than -24 PVU by 0600 UTC 2 January. This mesoscale intensification process through the inward transport of the rainband-induced cyclonic PV anomalies supports the hypothesis of May and Holland (1999). They estimated diabatic heating and PV generation in TC rainbands based on the observed vertical motion profiles and found high levels of PV generation in the stratiform rain regions. They suggested that such PV generation represents a significant PV source for the system as a whole as it is transported into the core and thus has implications for TC.

After the recovery of the quasi-symmetric structure of the inner-core PV, the simulated Isobel re-intensified and reached its lifetime maximum intensity by 0600 UTC 2 January. Again the storm gained the typical structure of a mature TC (Fig. 12), similar to the one during the intensifying stage discussed earlier (Fig. 10), but the storm now developed a deeper cyclonic circulation (Fig. 12c) and a larger horizontal size with a wider eyewall updraft (Fig. 12b). Accordingly, the azimuthal-mean diabatic heating rate in the eyewall occurred between radii of 30 and 60 km and in spiral rainbands around a radius of 100 km (Fig. 8e). The azimuthal-mean tangential wind tendency showed a large spinup in the eyewall in the mid-lower troposphere and immediately outside the eyewall in the mid-upper troposphere while a spindown in the eye region in the upper troposphere occurred (Fig. 12d), an indication of the development of an outward tilting of the radius of maximum wind (Fig. 12c).

The spinup of the primary circulation was mainly contributed by the mean transport of absolute angular momentum in the mid-lower troposphere in the inner-core region and in the eyewall (Fig. 12e) and by the eddy fluxes in the midtroposphere between radii of 50 and 150 km (Fig. 12f). The mean transport also contributed to the spinup of the tangential wind outer core with a maximum contribution between 7- and 10-km heights (Fig. 12e). Note that the eddy process contributed mainly to the tangential wind budget negatively (Fig. 12f) and thus played a role in weakening the storm intensity, consistent with the idealized simulation results of Yang et al. (2007). The Sawyer-Eliassen equation reproduced the secondary circulation well in the re-intensifying stage (Figs. 9e,f), indicating that the re-intensification of the simulated Isobel after the reformation of the eyewall and the recovery of the eyewall convection can be explained by the balanced dynamics, namely the SSI process again.

The inner-core cyclonic PV decreased after 1800 UTC 2 January as Isobel approached the northwest coast of Australia and continued to decay (Figs. 1 and 3). The azimuthal-mean diabatic heating rate became negligible in the inner-core region (Fig. 8f) and the weakening of the tangential winds started from the inner-core region (not shown). These changes overall are very similar to those in the temporary weakening stage.

5. A synthesis of the multiple-scale interaction in Isobel's life cycle

This study (i.e., Part I and Part II) documented both the external influence of the large-scale environmental flow on the structure and intensity changes and the involved mesoscale and system-scale processes in the life cycle of the simulated Isobel, as synthesized schematically in Figs. 13 and 14. The WWB associated with the onset of an MJO event over the Indian Ocean provided a favorable large-scale environmental condition for the genesis of Tropical Storm Isobel over the Java Sea (Fig. 13). This preconditioned environment was featured by strong large-scale cyclonic vorticity and convergence in the mid-lower troposphere and high CAPE. Convection was initiated and organized in a zonally elongated rainband with embedded MCSs near the cyclonic shear line in the preconditioned large-scale environment.

Some model MCVs with vorticity maxima in the midtroposphere developed in association with diabatic heating in stratiform clouds (Fig. 14a), consistent with previous finding of Raymond and Jiang (1990). Convective towers with cyclonic PV anomalies throughout the depth of the troposphere were initiated and developed in the MCVs (Fig. 14b). This featured the initial

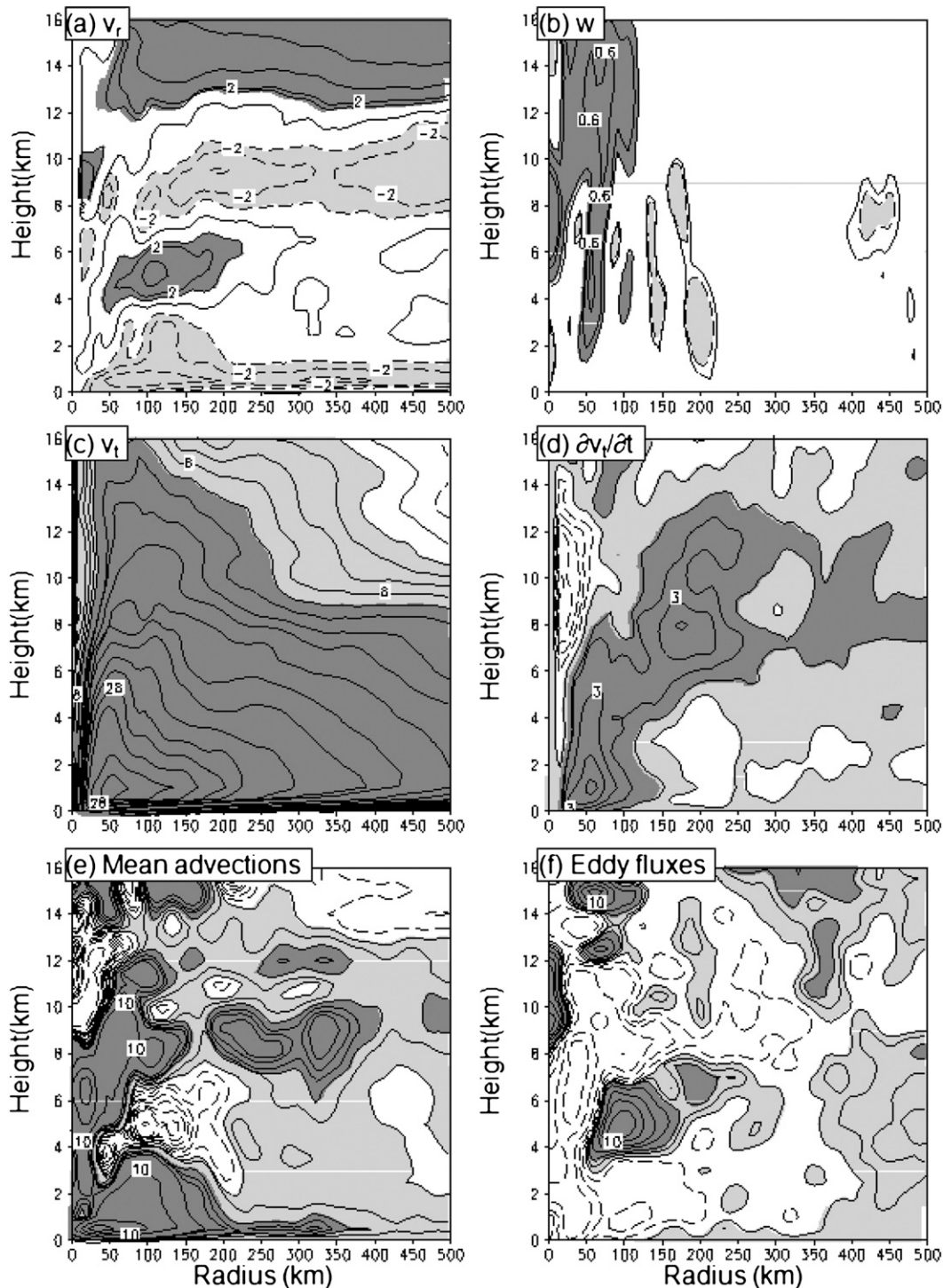


FIG. 12. As in Fig. 6, but at 0600 UTC 2 Jan 2007.

eddy stage of the simulated Isobel. Although it is difficult for us to examine the formation mechanisms of the convective vortices with a 7-km model resolution, the dipole PV structure with positive and negative PV

anomalies around the convective updraft in VHTs embedded in the merging MCVs (Fig. 5a) implies the importance of tilting of horizontal vorticity to the formation of VHTs (Montgomery et al. 2006). The MCVs provided

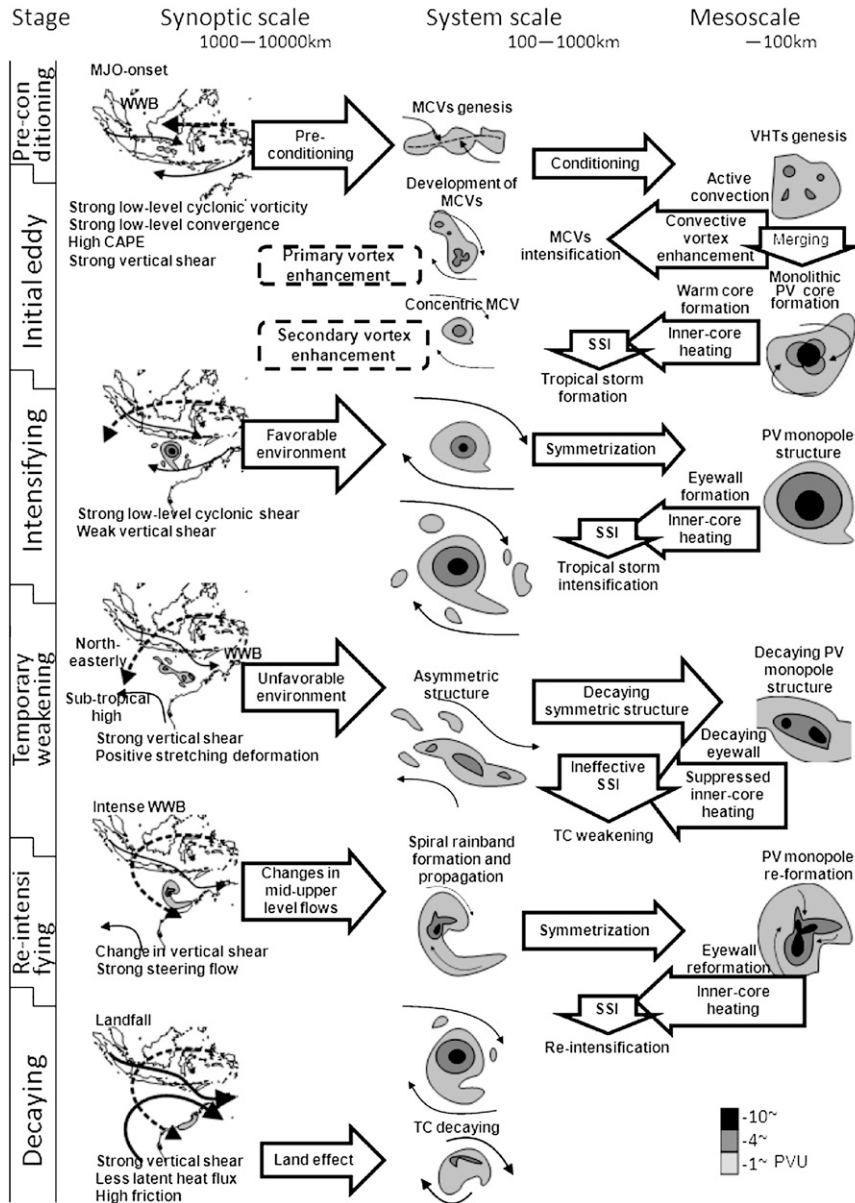


FIG. 13. Schematic diagram showing the vorticity evolution and the associated environmental flow on the (left) synoptic scale, (middle) system scale, and (right) mesoscale in the inner PV core. Regions with high cyclonic vorticity of -10 PVU are filled and regions with cyclonic vorticity of -4 PVU are heavily shaded, while regions with weak cyclonic vorticity of -1 PVU are lightly shaded. Solid arrows indicate the lower-level flow, while broken arrows show the upper-level flow.

necessary conditions for the formation of VHTs (Zhang and Fritsch 1987; Bartels and Maddox 1991; Zhang and Bao 1996a,b).

Multiple model VHTs merged and strengthened cyclonic PV anomaly in the interior of the merging MCV and led to the formation of an upright monolithic PV core at the center of concentric MCV (primary vortex enhancement; Fig. 14c), as discussed in Hendricks et al.

(2004), Montgomery et al. (2006), and Tory et al. (2006b). As the monolithic PV core with a warm core developed near the circulation center, the cyclonic PV was enhanced by the SSI process driven by diabatic heating in the inner-core region (secondary vortex enhancement; Fig. 14d). This was accompanied by the intensification and the increase in horizontal size of the cyclonic circulation, leading to the formation of Tropical Storm Isobel.

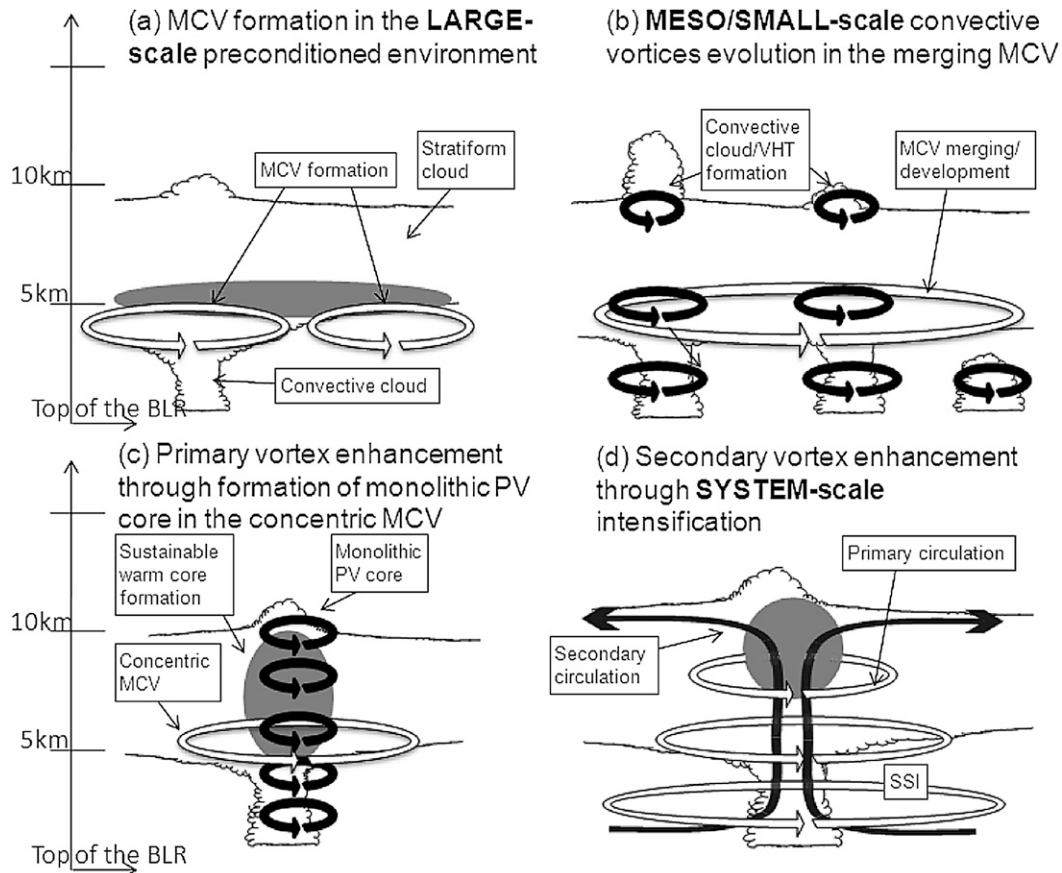


FIG. 14. Schematic diagram of the vertical cross section showing the genesis processes of (a) large-scale preconditioning, (b) meso/small-scale convective vortices evolution, (c) primary vortex enhancement, and (d) secondary vortex enhancement. Regions with significant diabatic heating are shaded, and cloud regions are schematically drawn. In (a)–(c), opened arrows indicate the MCV, while solid arrows show the convective vortex (VHT). In (d), opened arrows show the system-scale primary circulation, while solid arrows indicate the system-scale secondary circulation in response of the formed warm core. Note that the Northern Hemisphere motion is used for cyclonic rotation in the figure while Tropical Storm Isobel is a Southern Hemispheric tropical cyclone.

Although the azimuthal-mean secondary circulation contributed largely to the spinup of the primary circulation in the formation stage, eddy process also played a positive role in the upper and lower troposphere during the early genesis stage (Fig. 6f), consistent with the results of Hendricks et al. (2004).

In the intensifying stage, Isobel moved into the Timor Sea and continued to intensify under the favorable large-scale environment with weak vertical shear and strong low-level cyclonic shear (Fig. 13). The high cyclonic PV core intensified and became axisymmetric, and the eyewall formed with enhanced convective heating. The secondary circulation in response to diabatic heating in the eyewall accelerated the azimuthal-mean primary circulation through inward transport of absolute angular momentum. This intensification process (SSI) can be explained well by the balanced dynamics based on the

Sawyer–Eliassen equation with the eddy processes playing some secondary roles.

As the simulated Isobel moved southward and the MJO propagated eastward, Isobel was exposed to the region first with a strong vertical shear and later with a strong stretching deformation field upwind of the WWB in the MJO, leading to a breakdown of the eyewall and a temporary weakening of the storm (the temporary weakening stage). The weakening of the primary circulation occurred mainly in the inner core and started from the top down, consistent with previous results from idealized simulations in Frank and Ritchie (2001). This spin-down process was related to the strengthening and inward penetration of an inflow immediately below the upper-tropospheric outflow, the azimuthal-mean subsidence in

the inner-core region, and a deep outflow layer in the mid-lower troposphere above the inflow boundary layer. As convection in the eyewall was suppressed, the azimuthal-mean diabatic heating rate became negligible in the inner-core region, and the SSI process thus became ineffective and the storm weakened.

In the late temporally weakening stage, as the storm moved southeastward, the vertical shear changed from easterly shear to north-northeasterly shear over the inner core, leading to the development and intensification of a strong outer spiral rainband to the south-southeast of the storm center, namely downwind of the WWB center. The outer rainband propagated cyclonically inward and axisymmetrized, leading to the reformation of the eyewall and the reintensification of the simulated Isobel. Therefore, the eyewall reformation as a result of the axisymmetrization of the inward-propagating outer spiral rainbands was an important process to the reintensification of the simulated Isobel. The eyewall reformation was accompanied by recovery of a quasi-axisymmetric inner-core structure with enhanced azimuthal-mean diabatic heating in the eyewall, allowing the SSI process to operate effectively and the reintensification of the simulated Isobel. Note that although the axisymmetrization contributed to the reintensification, the latter might also be speeded up the axisymmetrization process of the inward-propagating spiral rainband and the reformation of the eyewall. As the simulated Isobel moved farther southeastward and approached the northwest coast of Australia, it weakened because of the continued decrease in moisture supply from the underlying ocean surface and eventually it dissipated after it made landfall over northwest Australia.

6. Conclusions

The life cycle of Tropical Storm Isobel was reasonably simulated in the global cloud-system-resolving model, NICAM. In this study, we have investigated both the large-scale and storm-scale evolutions (Part I) and the system-scale and mesoscale processes (Part II) in the life cycle of the simulated Isobel. As we have synthesized in the last section, the life cycle of the simulated Isobel involved multiscale interactions from cloud-scale convective activities to large-scale circulation related to the onset of MJO and the associated WWB. We show that the large-scale environmental flow provided the preconditioned environment for the genesis of the simulated Isobel and triggered the subsequent structure change of the storm. The mesoscale and the system-scale processes, such as the evolution of MCVs and merging VHTs were responsible for the genesis, while the eyewall processes were critical to the storm intensity change through the SSI process.

In the special case of Isobel, we have found that the WWB associated with the onset of a MJO event played dual roles in the life cycle of the simulated Isobel. On one hand, the WWB contributed positively to the intensification of Isobel as Isobel was located southeast of the WWB center where large-scale convergence occurred with high CAPE. On the other hand it contributed to the development of the asymmetric structure in the inner core and thus negatively to Isobel's intensification as Isobel was located southwest of the WWB center where the environmental stretching deformation was strong. Therefore, depending on the relative location of Isobel and the WWB center associated with the MJO, the MJO had both positive and negative effects on the intensity of the simulated Isobel. We thus suggest that caution needs to be given to the relative location between the WWB and the TC when the possible effect of the MJO on a TC is discussed.

In a simulation study of real TCs, Tory et al. (2006b) considered two processes for the genesis: the primary vortex enhancement through the convective vortex enhancement and the formation of PV core in convective updrafts (Hendricks et al. 2004; Montgomery et al. 2006) and the secondary vortex enhancement through the SSI process. Our results also demonstrate that both mesoscale and system-scale processes are critical to the genesis of the simulated Isobel in a preconditioned large-scale environment. We also show that the SSI process operates effectively only when the storm intensifies with intense convection in the inner-core region. The SSI process becomes ineffective when there is little azimuthal-mean diabatic heating in the inner core. This suggests that special attention should be paid to the eyewall process in order to understand and predict the structure and intensity changes of a TC.

Note that our results are based on NICAM MJO experiment at 7-km resolution, which could only marginally capture the important mesoscale processes in the life cycle of Isobel. This resolution is not high enough to examine the life cycle of individual VHTs and the statistical behavior of VHTs. Although now NICAM can be run at 3.5-km resolution for monthly long simulations, it is still not high enough to study convection in details. Therefore, studies with regional fine-resolution cloud-resolving models are still important for our understanding of the life cycle of TCs. Nevertheless, our case study for Isobel based on the NICAM simulation demonstrates the potential use of nearly cloud-resolving global models to study the life cycle of TCs.

In addition, as we pointed out already in Part I, although the NICAM MJO experiment provided us an opportunity to study the multiscale interactions involved in the life cycle of the simulated Isobel, the results do not

imply skill at monthly-long forecasting of TC behaviors. The timing and structure and intensity change were largely controlled by the large-scale environmental settings associated with the onset of an MJO event. Realistic simulation and prediction of the MJO are still challenging to most regional and global models (Sperber and Waliser 2008; Kim et al. 2009). Nevertheless, global cloud-system-resolving models have recently shown consistent improvements in the simulation of the MJO (Miura et al. 2007; Liu et al. 2009). Therefore, the extended realistic simulation and skillful prediction of TCs by numerical models are expected to be improved along with the continuous improvements in the ability of global models in simulating and predicting the tropical variability of convective activities at intraseasonal time scales.

Acknowledgments. The authors are grateful to the anonymous reviewers for their helpful comments. This study was supported in part by NSF Grant ATM-0754039 and in part by JAMSTEC, NASA, and NOAA through their sponsorships of the International Pacific Research Center (IPRC) in the School of Ocean and Earth Science and Technology (SOEST) at the University of Hawaii. Part of this study was also supported by the JST/CREST in Japan. The Earth Simulator was used for the NICAM simulations.

REFERENCES

- Bartels, D. L., and R. A. Maddox, 1991: Midlevel cyclonic vortices generated by mesoscale convective systems. *Mon. Wea. Rev.*, **119**, 104–118.
- Bister, M., and K. A. Emanuel, 1997: The genesis of Hurricane Guillermo: TEXMEX analyses and a modeling study. *Mon. Wea. Rev.*, **125**, 2662–2682.
- Eliassen, A., 1951: Slow thermally or frictionally controlled meridional circulation in a circular vortex. *Astrophys. Norv.*, **5**, 19–60.
- Fang, J., and F. Zhang, 2010: Initial development and genesis of Hurricane Dolly (2008). *J. Atmos. Sci.*, **67**, 655–672.
- , and —, 2011: Evolution of multiscale vortices in the development of Hurricane Dolly (2008). *J. Atmos. Sci.*, **68**, in press.
- Frank, W. M., and E. A. Ritchie, 2001: Effects of vertical wind shear on the intensity and structure of numerically simulated hurricanes. *Mon. Wea. Rev.*, **129**, 2249–2269.
- Fudeyasu, H., and Y. Wang, 2011: Contribution by balanced dynamics to the intensification of a tropical cyclone simulated in TCM4: Outer core spinup process. *J. Atmos. Sci.*, in press.
- , —, M. Satoh, T. Nasuno, H. Miura, and W. Yanase, 2008: Global cloud-system-resolving model NICAM successfully simulated the lifecycles of two real tropical cyclones. *Geophys. Res. Lett.*, **35**, L22808, doi:10.1029/2008GL036003.
- , —, —, —, —, and —, 2010: Multiscale interactions in the life cycle of a tropical cyclone simulated in a global cloud-system-resolving model. Part I: Large-scale and storm-scale evolutions. *Mon. Wea. Rev.*, **138**, 4285–4304.
- Hendricks, E. A., M. T. Montgomery, and C. A. Davis, 2004: The role of “vortical” hot towers in the formation of Tropical Cyclone Diana (1984). *J. Atmos. Sci.*, **61**, 1209–1232.
- Holland, G. J., and R. T. Merrill, 1984: On the dynamics of tropical cyclone structural changes. *Quart. J. Roy. Meteor. Soc.*, **110**, 723–745.
- Kim, D., and Coauthors, 2009: Application of MJO simulation diagnostics to climate models. *J. Climate*, **22**, 6413–6436.
- Liu, P., and Coauthors, 2009: An MJO simulated by the NICAM at 14- and 7-km resolutions. *Mon. Wea. Rev.*, **137**, 3254–3268.
- May, P. T., and G. J. Holland, 1999: The role of potential vorticity generation in tropical cyclone rainbands. *J. Atmos. Sci.*, **56**, 1224–1228.
- Miura, H., M. Satoh, T. Nasuno, A. T. Noda, and K. Oouchi, 2007: A Madden–Julian Oscillation event realistically simulated by a global cloud-resolving model. *Science*, **318**, 1763–1765.
- Montgomery, M. T., M. E. Nicholls, T. A. Cram, and A. B. Saunders, 2006: A vortical hot tower route to tropical cyclogenesis. *J. Atmos. Sci.*, **63**, 355–386.
- Ooyama, K., 1969: Numerical simulation of the life cycle of tropical cyclones. *J. Atmos. Sci.*, **26**, 3–40.
- Raymond, D. J., and H. Jiang, 1990: A theory for long-lived mesoscale convective systems. *J. Atmos. Sci.*, **47**, 3067–3077.
- Reasor, P. D., M. T. Montgomery, and L. F. Bosart, 2005: Mesoscale observations of the genesis of Hurricane Dolly (1996). *J. Atmos. Sci.*, **62**, 3151–3171.
- Ritchie, E. A., and G. J. Holland, 1997: Scale interactions during the formation of Typhoon Irving. *Mon. Wea. Rev.*, **125**, 1377–1396.
- Rotunno, R., and K. A. Emanuel, 1987: An air–sea interaction theory for tropical cyclones. Part II: Evolutionary study using a nonhydrostatic axisymmetrical numerical model. *J. Atmos. Sci.*, **44**, 542–561.
- Satoh, M., T. Matsuno, H. Tomita, H. Miura, T. Nasuno, and S. Iga, 2008: Nonhydrostatic icosahedral atmospheric model (NICAM) for global cloud resolving simulations. *J. Comput. Phys.*, **227**, 3486–3514.
- Schubert, W. H., and J. J. Hack, 1982: Inertial stability and tropical cyclone development. *J. Atmos. Sci.*, **39**, 1687–1697.
- Shapiro, L. J., and H. E. Willoughby, 1982: The response of balanced hurricanes to local sources of heat and momentum. *J. Atmos. Sci.*, **39**, 378–394.
- Simpson, J., E. Ritchie, G. J. Holland, J. Halverson, and S. Stewart, 1997: Mesoscale interactions in tropical cyclone genesis. *Mon. Wea. Rev.*, **125**, 2643–2661.
- Sippel, J. A., J. W. Nielsen-Gammon, and S. E. Allen, 2006: The multiple-vortex nature of tropical cyclogenesis. *Mon. Wea. Rev.*, **134**, 1796–1814.
- Sperber, K. R., and D. E. Waliser, 2008: New approaches to understanding, simulating, and forecasting the Madden–Julian oscillation. *Bull. Amer. Meteor. Soc.*, **89**, 1917–1920.
- Tomita, H., and M. Satoh, 2004: A new dynamical framework of nonhydrostatic global model using the icosahedral grid. *Fluid Dyn. Res.*, **34**, 357–400.
- Tory, K. J., M. T. Montgomery, and N. E. Davidson, 2006a: Prediction and diagnosis of tropical cyclone formation in an NWP system. Part I: The critical role of vortex enhancement in deep convection. *J. Atmos. Sci.*, **63**, 3077–3090.
- , —, —, and J. D. Kepert, 2006b: Prediction and diagnosis of tropical cyclone formation in an NWP system. Part II: A diagnosis of Tropical Cyclone Chris formation. *J. Atmos. Sci.*, **63**, 3091–3113.
- , N. E. Davidson, and M. T. Montgomery, 2007: Prediction and diagnosis of tropical cyclone formation in an NWP system.

- Part III: Diagnosis of developing and nondeveloping storms. *J. Atmos. Sci.*, **64**, 3195–3213.
- Wang, Y., 2002a: Vortex Rossby waves in a numerically simulated tropical cyclone. Part I: Overall structure, potential vorticity, and kinetic energy budgets. *J. Atmos. Sci.*, **59**, 1213–1238.
- , 2002b: Vortex Rossby waves in a numerically simulated tropical cyclone. Part II: The role in tropical cyclone structure and intensity changes. *J. Atmos. Sci.*, **59**, 1239–1262.
- , and C. C. Wu, 2004: Current understanding of tropical cyclone structure and intensity changes—A review. *Meteor. Atmos. Phys.*, **87**, 257–278.
- Willoughby, H. E., J. A. Clos, and M. G. Shoreibah, 1982: Concentric eye walls, secondary wind maxima, and the evolution of the hurricane vortex. *J. Atmos. Sci.*, **39**, 395–411.
- Yang, B., Y. Wang, and B. Wang, 2007: The effect of internally generated inner core asymmetric structure on tropical cyclone intensity. *J. Atmos. Sci.*, **64**, 1165–1188.
- Zhang, D. L., and J. M. Fritsch, 1987: Numerical simulation of the meso-beta scale structure and evolution of the 1977 Johnstown flood. Part II: Inertially stable warm-core vortex and the mesoscale convective complex. *J. Atmos. Sci.*, **44**, 2593–2612.
- , and N. Bao, 1996a: Oceanic cyclogenesis as induced by a mesoscale convective system moving offshore. Part I: A 90-h real-data simulation. *Mon. Wea. Rev.*, **124**, 1449–1469.
- , and —, 1996b: Oceanic cyclogenesis as induced by a mesoscale convective system moving offshore. Part II: Genesis and thermodynamic transformation. *Mon. Wea. Rev.*, **124**, 2206–2225.